APL MATERIALS **2**, 092802 (2014)

Characterization of few-layer 1T-$MoSe_2$ and its superior performance in the visible-light induced hydrogen evolution reaction

Uttam Gupta,[1] B. S. Naidu,[1] Urmimala Maitra,[1] Anjali Singh,[2]
Sharmila N. Shirodkar,[2] Umesh V. Waghmare,[2] and C. N. R. Rao[1,a]
[1]*Chemistry and Physics Materials Unit, New Chemistry Unit and International Centre for Materials Science, Sheik Saqr Laboratory, Jawaharlal Nehru Centre for Advanced Scientific Research, Jakkur P. O., Bangalore 560064, India*
[2]*Theoretical Sciences Unit, Jawaharlal Nehru Centre for Advanced Scientific Research, Jakkur P. O., Bangalore 560064, India*

(Received 23 March 2014; accepted 1 August 2014; published online 2 September 2014)

Based on earlier results on the photocatalytic properties of MoS_2, the 1T form of $MoSe_2$, prepared by lithium intercalation and exfoliation of bulk $MoSe_2$, has been employed for the visible-light induced generation of hydrogen. 1T-$MoSe_2$ is found to be superior to both 2H and 1T MoS_2 as well as 2H-$MoSe_2$ in producing hydrogen from water, the yield being in the 60–75 mmol h^{-1} g^{-1} range with a turn over frequency of 15–19 h^{-1}. First principles calculations reveal that 1T-$MoSe_2$ has a lower work function than 2H-$MoSe_2$ as well as 1T and 2H-MoS_2, making it easier to transfer an electron from 1T-$MoSe_2$ for the production of H_2. [http://dx.doi.org/10.1063/1.4892976]

Artificial photosynthesis has been recognized as a potential means of water splitting. Various strategies which can be employed for this purpose like dye sensitization of semiconductors or use of light-harvesting semiconducting nanostructures. TiO_2 was the first material to be used as the photocatalyst for water-splitting.[1] Since then several inorganic catalysts have been used for photocatalytic, photoelectrochemical, and electrocatalytic production of H_2 from water. Semiconducting oxide nanoparticles are one of the most common photocatalysts used for this purpose[2,3] and are preferred because they are chemically robust and stable against photocorrosion during water splitting. The intrinsic limitation of oxides is that they generally have a highly positive valence band (O 2*p*), making it difficult to find a material which has both sufficiently negative conduction band to reduce H_2O to H_2 along with a sufficiently small bandgap to absorb visible light.[4,5] Metal sulfides and selenides, on the other hand, have less positive valence bands making them visible light active. Majority of the metal sulfides however undergo photocorrosion during the hydrogen evolution reaction (HER).

Transition metal dichalcogenides of lamellar structure have gained attention recently because of their interesting electronic properties and easy availability.[6,7] Exfoliation of these materials into single or few-layers often brings about drastic changes in the electronic structure as compared to the bulk species. Dichalcogenides of MoS_2 and WS_2 generally occur in the 2H form with the trigonal prismatic arrangement of hexagonal S–M–S (M = Mo/W) triple layers are among the most studied of the layered metal chalcogenides. While the 2H forms of these metal dichalcogenides are semiconducting, the 1T forms are metallic.[8–10] MoS_2 has been widely used as a catalyst for electrochemical, photoelectrochemical, and photocatalytic H_2 generation from water[11–14] in consequence of having the conduction band minimum well above the H_2O reduction potential.[15–17] Nanoparticles of 2H-MoS_2 as well as composites of 2H-MoS_2 with graphene and other materials have been employed as

[a]Author to whom correspondence should be addressed. Electronic mail: cnrrao@jncasr.ac.in

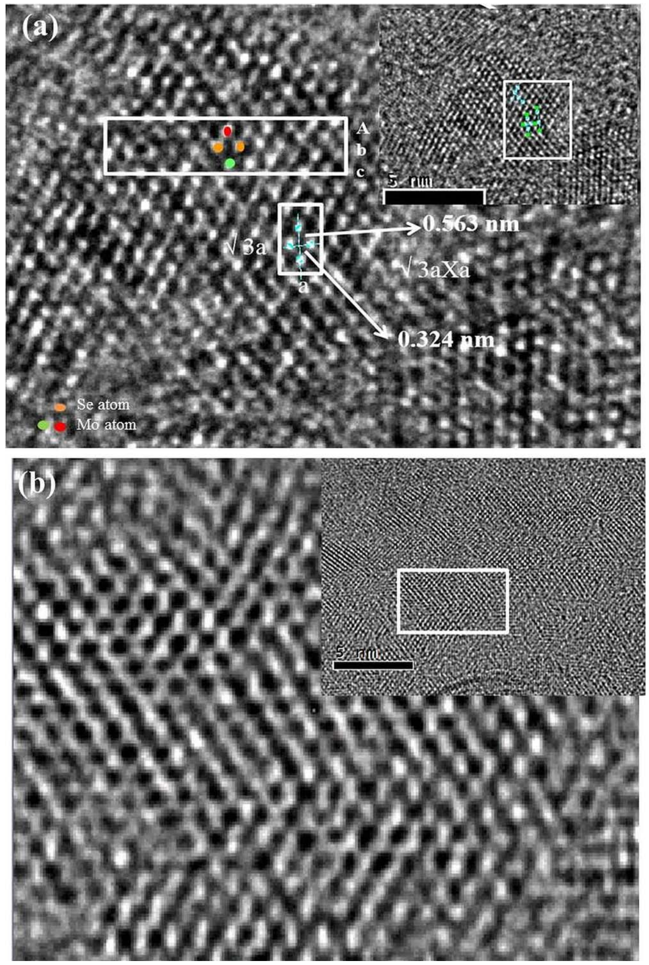

FIG. 1. HRTEM of (a) 1T-$MoSe_2$ and (b) 2H-$MoSe_2$.

catalysts yielding 0.05–10 mmol h^{-1} g^{-1} of H_2 with a turn over frequency anywhere between 0.2 and 6 h^{-1}.[13,18–21] It has been shown recently that the composite of MoS_2 with heavily nitrogen-doped graphene has an activity of 10.8 mmol h^{-1} g^{-1} and a turn over frequency of 2.9 h^{-1} under a 100 W halogen lamp.[21] This was further improved by using 1T-MoS_2 prepared by the exfoliation of bulk MoS_2 by Li-intercalation. The metallic nature of 1T MoS_2 is expected to be responsible for H_2 evolution.[21–23] 2H-$MoSe_2$ with an indirect bandgap of 1.05 eV has its conduction band minimum 0.37 eV higher than 2H-MoS_2, and well above the water reduction potential,[15,16] thereby making it an ideal catalyst for H_2 evolution. The 1T form of $MoSe_2$ is also metallic and could be expected to be a better catalyst than its 2H analogue for water reduction. Based on these findings, we have exfoliated bulk 2H-$MoSe_2$ after Li-intercalation to obtain few-layer 1T-$MoSe_2$ with the octahedral co-ordination of Mo[22] and employed it for HER by under visible light. We find that 1T-$MoSe_2$ is superior to 2H-$MoSe_2$ as well as 1T-MoS_2.

Bulk $MoSe_2$ in the 2H form was intercalated with lithium using n-butyl lithium and exfoliation carried out by reacting the intercalated product with water.[24–26] The high resolution transmission electron microscope image in Fig. 1(a) shows that the exfoliated sample corresponds to the 1T phase with an octahedral (O_h) or trigonal antiprismatic symmetry. The 1T form has the $\sqrt{3}a \times a$ arrangement which is related to its electronic structure.[25,27] The shifting of the atoms from their equilibrium positions, probably arises because of the Jahn-Teller instability, resulting in chain clusterization of the metal atoms with the formation of a superlattice.[28] This distorted phase is stable as a dispersion in water even after Li is removed, but restacks when dried,[21] to transform

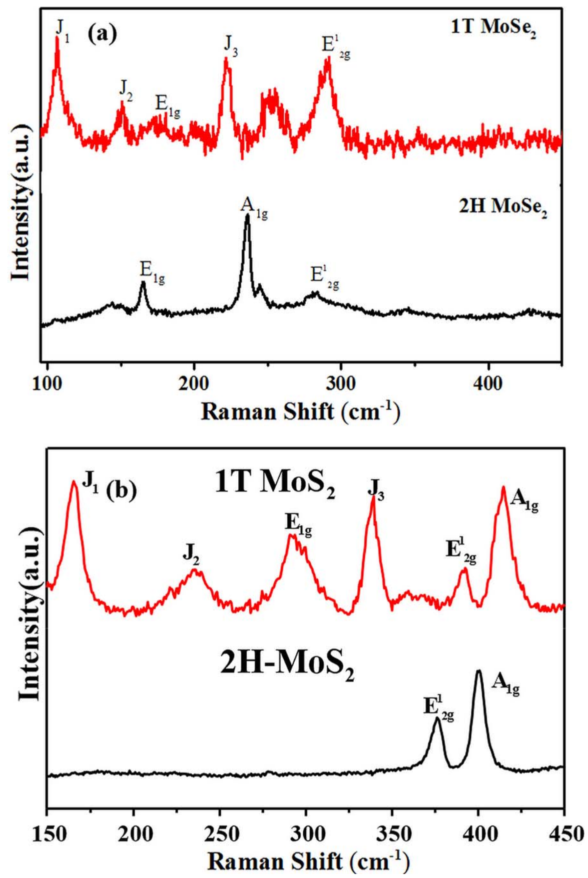

FIG. 2. Comparison of Raman spectra of (a) 1T-$MoSe_2$ and 2H-$MoSe_2$ and (b) 1T-MoS_2 and 2H-MoS_2.

TABLE I. Raman modes of 1T and 2H forms of $MoSe_2$ and MoS_2.

Raman modes	2H $MoSe_2$ (cm^{-1})	2H MoS_2 (cm^{-1})	1T-$MoSe_2$ (cm^{-1})	1T-MoS_2 (cm^{-1})	$MoSe_2$ bulk (cm^{-1})
J_1	...	...	106.4	165.4	...
J_2	...	...	150.7	236.6	...
J_3	...	...	221.4	339.3	...
A_{1g}	236.2	400	...	414.3[a]	240.1
E_{1g}	165		...	292.4	166.7
$E^1{}_{2g}$		375.9	289.4	391.3	...

[a]Some 2H contribution.

into thermodynamically stable 2H phase. The Mo atoms in the 2H form of $MoSe_2$ have trigonal prismatic coordination as is evident from the high resolution TEM image in Fig. 1(b). The packing of atoms in 2H $MoSe_2$ is AbA type while in the 1T form it is AbC type. The point group of the trigonal prismatic 2H-$MoSe_2$ is D_{3h} while the 1T polytype belongs to the D_{3d} point group.[24] The 1T phases of both $MoSe_2$ and MoS_2 exhibit a Raman spectra which are distinctly different from those of the 2H-phases. In Fig. 2, we show the Raman spectra of the 1T phases of $MoSe_2$ and MoS_2 and compare them with the spectra of the 2H phases. We list the band positions of these phases in Table I.

Bulk (2H) $MoSe_2$ has d^2 electronic configuration and hexagonal (D_{3h}) symmetry which would induce splitting of the 4*d* orbitals into three orbitals of closely spaced energies (shown in Fig. 3(a) (i)). The Mo $4d_z{}^2$ level is occupied and spin paired forming the valence band minimum (VBM), while the other four orbitals form the empty conduction band. During lithium intercalation, a structural re-orientation occurs to the stable half-filled *d*-orbital configuration in the octahedral

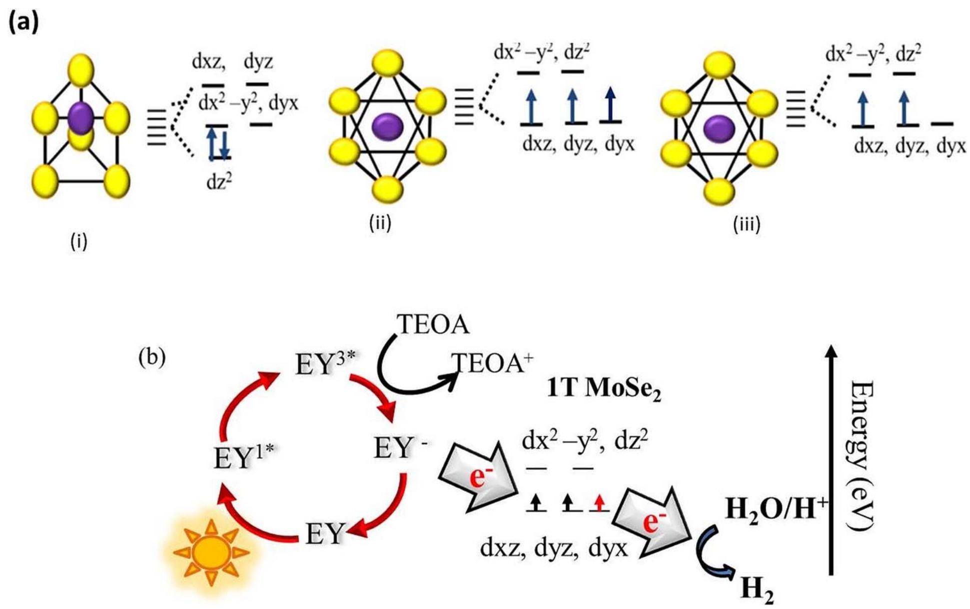

FIG. 3. (a) The crystal field induced electronic configuration of (i) 2H- $MoSe_2$, (ii) Li-intercalated $MoSe_2$, and (iii) 1T-form and (b) the plausible mechanism of HER.

geometry (D_{3d}) as shown in Fig. 3(a) (ii) which is responsible for the Mo atoms to go from the prismatic co-ordination to the anti-prismatic co-ordination in the 1T-form. Addition of water causes an exothermic reaction because of which the $MoSe_2$ sheets get separated and remain in this metastable 1T-form. The crystal-field splitting of Mo 4*d* under the octahedral O_h field generates two set of degenerate orbitals as shown in Fig. 3(a) (iii). The incompletely filled d_{yx}, d_{zx}, d_{zy} orbital gives rise to the metallic properties of 1T-$MoSe_2$. The Fermi level in 1T-$MoSe_2$ therefore lies in the Mo 4*d* making it metallic. Based on the electronic configuration of 1T and 2H phases of $MoSe_2$ it is clear that when an extra electron is added to 2H-$MoSe_2$, it resides in the degenerate d_{yx}, $d_{x^2-y^2}$ states and destabilizes the lattice, while in case of 1T-$MoSe_2$ the extra electron induces half-filled configuration of d_{yx}, d_{zx}, d_{zy} and increases the stability of the 1T phase.

The hydrogen evolution activity of 1T-$MoSe_2$ was studied using Eosin Y as the sensitizer and triethanolamine as the sacrificial electron donor. The reaction of dye-sensitized H_2 evolution over $MoSe_2$ involves photosensitization of Eosin Y followed by formation of Eosin Y anion (EY^-). EY^- being highly reactive donates this electron to $MoSe_2$, which then catalyzes the reduction of proton to H_2 as shown in Fig. 3(b). Fig. 4 shows the time course of hydrogen evolution by 1T $MoSe_2$. The yields are in range of the 60–75 mmol g^{-1} h^{-1} and remains the same at least up to 5 cycles, i.e., 30 h, with 0.014 mM of dye being added after each cycle (see Fig. S2 of the supplementary material).[29] The turn over frequencies (TOF) are in the range 15–19 h^{-1}. The catalytic activity of the 1T form of $MoSe_2$ is nearly few hundred times higher than that of the 2H form (see inset of 4(a)). It is noteworthy that the yield of H_2 and TOF with 1T-$MoSe_2$ is superior even to those found with 1T MoS_2. The 2H form of $MoSe_2$ too shows better activity than that of 2H-MoS_2 (yield of 0.05 mmol g^{-1} h^{-1} and TOF of 0.008 h^{-1}). In Table II, we have compared the hydrogen evolution activity and TOF of different transition metal chalcogenides. 1T-$MoSe_2$ shows higher activity compared to these transition metal chalcogenides and their composites. 1T forms of other metallic transition metal sulfides like TaS_2 and TiS_2 have earlier been shown to be active co-catalysts for H_2 evolution.[30] However, the activity for H_2 evolution is much lower in these chalcogenides as compared to 1T-MoS_2[21] and 1T-$MoSe_2$. Greater stability afforded by the extra electron to Mo 4*d* level by inducing a half-filled configuration of d_{yx}, d_{zx}, d_{zy}, as compared to Ta 5*d* (with 1 electron) and Ti 3*d* (with no electron) is probably the reason for higher activity of 1T-MoS_2 and 1T-$MoSe_2$.

It is worthwhile to note that $MoSe_2$ shows H_2 evolution on sensitization with dye. It may therefore not be considered to be a photocatalyst similar to TiO_2, where photo-excited electrons

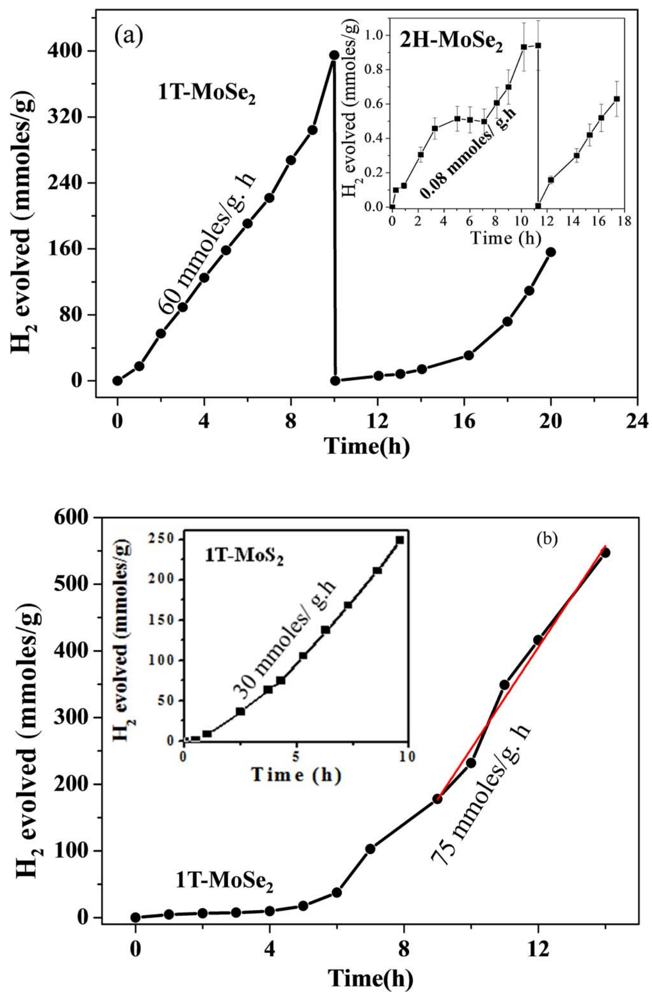

FIG. 4. Time course of H_2 evolution by two independently prepared 1T-$MoSe_2$ shown in (a) and (b). Inset in (a) shows the performance of 2H-$MoSe_2$ and in (b) of 1T-MoS_2 Reprinted with permission from U. Maitra, U. Gupta, M. De, R. Datta, A. Govindaraj, and C. N. R. Rao, Angew. Chem. Int. Ed. 52, 13057–13061 (2013). Copyright 2013 WILEY-VCH Verlag GmbH & Co. KGaA, Weinheim.[21] The slow reaction initially in (b) is due to the slow mixing of the reactants arising from the syrupy nature of triethanol amine.

TABLE II. Hydrogen evolution activity of $MoSe_2$, MoS_2, and TaS_2 based catalysts from earlier literature and present work. TOF calculated per mole of catalytically active material (graphene is considered to be inactive compared to MoS_2).

Compounds	Light source	Activity (mmol h^{-1} g^{-1})	TOF (h^{-1})	Reference
MoS_2/CdS	300 W Xe lamp	5.3	∼0.7	20
TaS_2/CdS	400 W Xe lamp ($\lambda > 399$ nm)	2.32	0.57	30
2H MoS_2[a]	100 W halogen lamp	0.05	0.008	21
NRGO-MoS_2[a]	100 W halogen lamp	10.8	2.9	21
1T MoS_2[a]	100 W halogen lamp	30	6.5	21
1T-$MoSe_2$[a]	100 W halogen lamp	62 ± 5	15.5 ± 2	Present work
Few layer 2H $MoSe_2$[a]	100 W halogen lamp	0.08	0.02	Present work

[a]Eosin Y dye sensitized.

directly reduce H_2O. $MoSe_2$ is still different from co-catalysts like Pt which show H_2 evolution in the presence of another catalyst like TiO_2 and cannot evolve H_2 from water even on sensitization with a dye. Conduction Band Minimum of $MoSe_2$ is favourable for HER but cannot generate enough photoelectrons by absorption of visible light (the bandgap being very small). The dye

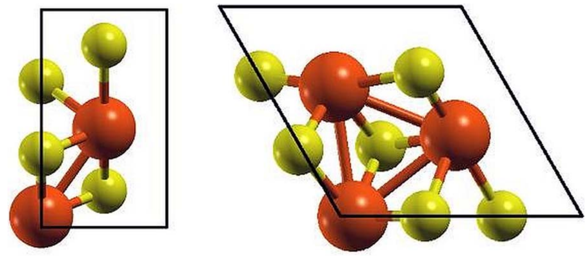

FIG. 5. $\sqrt{3} \times 1$ and $\sqrt{3} \times \sqrt{3}$ superstructures of 1T-MoX_2 (where X = S and Se). (a) $\sqrt{3} \times 1$ superstructure of 1T-MoX_2 showing dimerization of Mo atoms. (b) $\sqrt{3} \times \sqrt{3}$ superstructure of 1T-MoX_2 showing trimerization of Mo atoms. Mo atoms are shown in orange color and X atoms are in yellow.

donates an electron to $MoSe_2$ and induces the H_2 evolution reaction. We must point out that the exfoliated sample on restacking loses activity due to partial conversion to 2H-form. On annealing it transforms completely to the 2H form, thereby losing its hydrogen evolution activity (see Fig S3 of the supplementary material).[29]

In order to understand the higher activity of 1T-$MoSe_2$ in comparison to 2H-$MoSe_2$ and the 1T and 2H forms of MoS_2, we have carried out first-principles calculations based on density functional theory as implemented in Quantum ESPRESSO package,[31] in which the ionic and core-valence electron interactions are modeled with ultrasoft pseudopotentials.[32] The exchange-correlation energy of electrons is treated within a Generalized Gradient Approximation (GGA) functional as parametrized by Perdew, Burke, and Ernzerhof.[33] We use an energy cutoff of 35 Ry to truncate the plane wave basis used in representing the Kohn-Sham wave functions, and an energy cutoff of 280 Ry to represent the charge density. Structures are relaxed till the Hellman-Feynman forces on each atom are less than 0.02 eV/Å. We have used a periodic supercell geometry to simulate a 2D sheet, including vacuum of 15 Å to separate the adjacent periodic images of the sheet. For self-consistent Kohn-Sham (scf) calculations, configurations of $\sqrt{3} \times \sqrt{3}$ and $\sqrt{3} \times 1$ supercells, the BZ integrations are sampled over uniform meshes of $7 \times 7 \times 1$ and $12 \times 7 \times 1$ k-points, respectively. Since KS-DFT typically underestimates electronic bandgaps (a known limitation), we employ hybrid functional based on Hartree-Fock-Exchange (HSE)[34] with screened Coulomb potential to estimate the bandgaps more accurately. The calculations were based on first-principles DFT using Projector Augmented Wave (PAW) method[35,36] as implemented in the VASP (Vienna *Ab-initio* Simulations Package).[37] We have studied two superstructures of 1T-MoX_2 (where X = S and Se), $\sqrt{3} \times \sqrt{3}$ and $\sqrt{3} \times 1$[26] (Fig. 5). Among the two superstructures, $\sqrt{3} \times 1$ is metallic and shows dimerization of Mo atoms, and $\sqrt{3} \times \sqrt{3}$ is semiconducting with trimerized Mo atoms. From phonon dispersion, we find that, both MoS_2 and $MoSe_2$ are stable in the $\sqrt{3} \times \sqrt{3}$ and $\sqrt{3} \times 1$ superstructures. However, MoS_2 is energetically more stable in the $\sqrt{3} \times \sqrt{3}$ compared to $\sqrt{3} \times 1$ by 27 meV/f.u., while the $\sqrt{3} \times 1$ super-structure of $MoSe_2$ is energetically more stable than the $\sqrt{3} \times \sqrt{3}$ super-structure by 33 meV/f.u.

Experimentally, $MoSe_2$ is found to be in the $\sqrt{3} \times 1$ super-structure, in agreement with our first-principles results. Henceforth, we shall consider the $\sqrt{3} \times \sqrt{3}$ superstructure for MoS_2 and $\sqrt{3} \times 1$ superstructure for $MoSe_2$. To determine the efficiency of MoX_2 in reducing a proton to hydrogen as observed in experiments, we have estimated their electron affinities (EA) and work function (φ). For metallic states, the relevant property here is the work function. The EA is estimated as the difference between the vacuum potential (E_{vac}) and the lowest energy conduction band (E_{CB}). Since DFT is a ground state theory, estimation of the bandgap and hence the E_{CB} is not accurate. Hence, we replace the E_{CB} with $E_{VB} + E_g$, where E_{VB} is the energy of the highest energy valance band and E_g is the bandgap. Since E_g is grossly underestimated in DFT calculations, we use the HSE corrections (using VASP) to determine E_g accurately. For the monolayered MoS_2, experimental value of bandgap (1.8 eV[6]) is available.

Comparison of the experimental bandgap with calculated bandgap for 2H-MoS_2 reveals that Kohn-Sham bandgap is underestimated by 7.2% and the HSE bandgap is overestimated by 17.7% (see Table III), in agreement with Ahuja *et al.*[38] It is thus clear that the HSE method overestimates

TABLE III. The calculated and experimental values of bandgaps for 2H and 1T ($\sqrt{3} \times \sqrt{3}$ superstructure) structures of MoX_2 (MoS_2 and $MoSe_2$). HSE and KS-DFT bandgaps are calculated using VASP.

Compounds	Bandgap (eV) KS-DFT (VASP)	HSE (VASP)	Expt.
2H-MoS_2	1.67	2.12	1.8[34]
2H-$MoSe_2$	1.45	1.88	
1T-MoS_2 ($\sqrt{3} \times \sqrt{3}$)	0.76	1.28	
1T-$MoSe_2$($\sqrt{3} \times \sqrt{3}$)	0.64	1.16	

TABLE IV. The calculated values of electron affinity (EA) and work function (WF) for 1T (for both $\sqrt{3} \times \sqrt{3}$ and $\sqrt{3} \times 1$ superstructures) and 2H structures of MoX_2 (MoS_2 and $MoSe_2$).

Superstructure	1T-form $\sqrt{3} \times \sqrt{3}$		1T-form $\sqrt{3} \times 1$		2H-form	
Compound	MoS_2	$MoSe_2$	MoS_2	$MoSe_2$	MoS_2	$MoSe_2$
EA (eV)	4.95	4.42	...	...	4.22	3.78
WF (eV)	5.68	5.20	5.63	5.00	5.86	5.35

the experimental bandgap, whereas the KS-DFT calculation (GGA) yields a better estimate. We use estimates of Eg obtained from KS-DFT calculations in this work. The work function for metals and semiconductors is calculated as $\varphi = E_{vac} - E_F$ (where E_F = Fermi energy) and $\varphi = E_{vac} - E_{VB}$ respectively. We find that (a) the 2H and 1T-polytypes of MoS_2 have a greater φ than that of the respective structure of $MoSe_2$ (refer to Table IV). This implies that it is easier to extract an electron from $MoSe_2$ compared to that of MoS_2 in both 1T and 2H polytypes. (b) The 1T polytype has a lower φ than that of 2H, which means that it is easier for the 1T to donate electron compared to the 2H-structure. This explains why the 1T-polytype of $MoSe_2$ produces hydrogen more efficiently than the 2H-polytype as observed in experiments. The electron affinities of both 1T and 2H polytypes indicate that MoS_2 has a stronger electron affinity (indicating a higher tendency to attract electrons) than that of $MoSe_2$ (refer to Table IV), and the work function is also larger for MoS_2. Thus, though MoS_2 more readily attracts/accepts electrons, it does not donate it that easily. Hence, $MoSe_2$ is efficient in hydrogen evolution as compared to that of MoS_2 as observed in experiments here.

To connect the hydrogen (H) binding energy to the catalytic activity of the MoX_2 compounds, we have determined the binding energy of hydrogen (H) to $\sqrt{3} \times 1$ 1T superstructure of MoS_2 and $MoSe_2$. This superstructure is relevant to the experiments reported here, and has the lowest work function.

The hydrogen binding energy is calculated as

$$E_{ads} = \frac{1}{n}\left[E\left(slab + nH\right) - E\left(slab\right) - \frac{n}{2}E\left(H_2\right)\right],$$

where n is the number of H atoms considered in the simulation.

Bulk MoS_2 and $MoSe_2$ do not absorb hydrogen ($E_{ads} > 0$). It has been reported that edges of these dichalcogenides are catalytically active in hydrogen adsorption.[22] We have therefore simulated ribbons of MoX_2 with two different types of edges (Mo terminated edge and X terminated edge), and their interaction with H (with 100% H coverage at the edges). The hydrogen binding energies at Mo sites at the edges of MoS_2 and $MoSe_2$ are −33.8 meV/f.u. and −32.3 meV/f.u., respectively. The respective Mo–H bond lengths are 1.72 Å and 1.73 Å. The hydrogen binding energies at the S/Se edges of MoS_2 and $MoSe_2$ are −34.6 meV/f.u. and −13.1 meV/f.u. respectively. The corresponding X–H bond lengths are 1.35 Å and 1.48 Å. The binding energy of hydrogen at the metal edge is about the same in the two compounds but the Se edge shows weaker binding with hydrogen than the S edge. According to the volcano plot,[39,40] this suggests a higher exchange current for hydrogen evolution over $MoSe_2$ compared to MoS_2. This is consistent with our analysis based on the work functions. Since $MoSe_2$ has a lower work function than MoS_2, its Fermi energy (E_F) lies closer to the normal hydrogen electrode (E_{NHE}), which allows an easy exchange of an electron with $MoSe_2$ (H atom has a weaker binding at the Se edge) as compared to MoS_2. Thus, $MoSe_2$ is more efficient in facilitating the hydrogen evolution reaction.

In conclusion, metallic 1T-$MoSe_2$ prepared by Li intercalation followed by exfoliation of bulk 2H-$MoSe_2$ shows excellent H_2 evolution activity in comparison to few-layered semiconducting 2H-$MoSe_2$. Interestingly, 1T-$MoSe_2$ shows better H_2 evolution activity than 1T-MoS_2 as well. Our first-principles analysis reveals that $MoSe_2$ has a lower work function as compared to MoS_2, and that the 1T-structure exhibits lower work function than the 2H-structure for both MoX_2 (X = S, Se). This results in easy transfer of electron from the $MoSe_2$ for the reduction to hydrogen, and hence $MoSe_2$ is more efficient for hydrogen evolution reaction compared to MoS_2, and in agreement with the experimental results.

[1] A. Fujishima and K. Honda, Nature (London) **238**, 37–38 (1972).
[2] R. Abe, J. Photochem. Photobiol. C: Photochem. Rev. **11**, 179–209 (2010).
[3] A. Kudo and Y. Miseki, Chem. Soc. Rev. **38**, 253–278 (2009).
[4] J. G. Yu, L. F. Qi, and M. Jaroniec, J. Phys. Chem. C **114**, 13118–13125 (2010).
[5] X. Chen and S. S. Mao, Chem. Rev. **107**, 2891–2959 (2007).
[6] K. F. Mak, C. Lee, J. Hone, J. Shan, and T. F. Heinz, Phys. Rev. Lett. **105**, 136805 (2010).
[7] A. Splendiani, L. Sun, Y. Zhang, T. Li, J. Kim, C. Chim, G. Galli, and F. Wang, Nano Lett. **10**, 1271–1275 (2010).
[8] F. Wypych, Th. Weber, and R. Prins, Chem. Mater. **10**, 723–727 (1998).
[9] A. N. Enyashin, L. Yadgarov, L. Houben, I. Popov, M. Weidenbach, R. Tenne, M. Bar-Sadan, and G. Seifert, J. Phys. Chem. C **115**, 24586–24591 (2011).
[10] C. Rovirat and M. Whangbo, Inorg. Chem. **32**, 4094–4097 (1993).
[11] X. Zong, Y. Na, F. Wen, G. Ma, J. Yang, D. Wang, Y. Ma, M. Wang, L. Sun, and C. Li, Chem. Commun. 4536–4538 (2009).
[12] Q. Xiang, J. Yu, and M. Jaroniec, J. Am. Chem. Soc. **134**, 6575–6578 (2012).
[13] X. Zong, H. Yan, G. Wu, G. Ma, F. Wen, L. Wang, and C. Li, J. Am. Chem. Soc. **130**, 7176–7177 (2008).
[14] J. Yang and H. S. Shin, J. Mater. Chem. A **2**, 5979–5985 (2014).
[15] H. Jiang, J. Phys. Chem. C **116**, 7664–7671 (2012).
[16] J. Kang, S. Tongay, J. Zhou, J. Li, and J. Wu, Appl. Phys. Lett. **102**, 012111 (2013).
[17] M. A. Lukowski, A. S. Daniel, C. R. English, F. Meng, A. Forticaux, R. J. Hamers, and S. Jin, Energy Environ. Sci. **7**, 2608–2613 (2014).
[18] Q. Ding, F. Meng, C. R. English, M. Caban-Acevedo, M. J. Shearer, D. Liang, A. S. Daniel, R. J. Hamers, and S. Jin, J. Am. Chem. Soc. **136**, 8504–8507 (2014).
[19] F. A. Frame and F. E. Osterloh, J. Phys. Chem. C **114**, 10628–10633 (2010).
[20] X. Zong, G. Wu, H. Yan, G. Ma, J. Shi, F. Wen, L. Wang, and C. Lee, J. Phys. Chem. C **114**, 1963–1968 (2010).
[21] U. Maitra, U. Gupta, M. De, R. Datta, A. Govindaraj, and C. N. R. Rao, Angew. Chem. Int. Ed. **52**, 13057–13061 (2013).
[22] A. M. Lukowski, A. S. Daniel, F. Meng, A. Forticaux, L. Li, and S. Jin, J. Am. Chem. Soc. **135**, 10274–10277 (2013).
[23] D. Voiry, H. Yamaguchi, J. Li, R. Silva, D. C. B. Alves, T. Fujita, M. Chen, T. Asefa, V. B. Shenoy, G. Eda, and M. Chhowalla, Nat. Mater. **12**, 850–855 (2013).
[24] S. J. Sandoval, D. Yang, R. F. Frindt, and J. C. Irwin, Phys. Rev. B **44**, 3955–3962 (1991).
[25] J. Heising and M. G. Kanatzidis, J. Am. Chem. Soc. **121**, 11720–11732 (1999).
[26] R. A. Gordon, D. Yang, E. D. Crozier, D. T. Jiang, and R. F. Frindt, Phys. Rev. B **65**, 125407 (2002).
[27] J. A. Wilson, F. J. Di Salvo, and S. Mahajan, Adv. Phys. **24**, 117–201 (1975).
[28] A. H. C. Neto, Phys. Rev. Lett. **86**, 4382–4385 (2001).
[29] See supplementary material at http://dx.doi.org/10.1063/1.4892976 for details of synthesis, characterization, and photocatalytic measurements.
[30] U. Gupta, B. G. Rao, U. Maitra, B. E. Prasad, and C. N. R. Rao, Chem. Asian J. **9**(5), 1311–1315 (2014).
[31] P. Giannozzi *et al.*, J. Phys.: Condens. Matter **21**, 395502 (2009).
[32] D. Vanderbilt, Phys. Rev. B **41**, 7892–7895 (1990).
[33] J. P. Perdew, K. Burke, and M. Ernzerhof, Phys. Rev. Lett. **77**, 3865–3868 (1996).
[34] J. Heyd, G. E. Scuseria, and M. Ernzerhof, J. Chem. Phys. **118**, 8207–8215 (2003).
[35] P. E. Blöchl, Phys. Rev. B **50**, 17953–17979 (1994).
[36] G. Kresse and D. Joubert, Phys. Rev. B **59**, 1758–1775 (1999).
[37] G. Kresse and J. Furthmüller, Phys. Rev. B **54**, 11169–11186 (1996).
[38] Y. Li, Y. Li, C. M. Araujo, W. Luo, and R. Ahuja, Catal. Sci. Technol. **3**, 2214–2220 (2013).
[39] J. K. Nørskov, J. K. Nørskov, T. Bligaard, A. Logadottir, J. R. Kitchin, J. G. Chen, S. Pandelov, and U. Stimming, J. Electrochem. Soc. **152**, J23–J26 (2005).
[40] A. B. Laursen, S. Kegnæs, S. Dahl, and I. Chorkendorff, Energy Environ. Sci. **5**, 5577–5591 (2012).